DOI: 10.1002/ejic.201001152

Comparing the Reactivity of Benzenedithiolate- versus Alkyldithiolate-Bridged $Fe_2(CO)_6$ Complexes with Competing Ligands

Daniel Streich,[a] Michael Karnahl,[a] Yeni Astuti,[a] Clyde W. Cady,[a] Leif Hammarström,[a] Reiner Lomoth,*[a] and Sascha Ott*[a]

Keywords: Enzyme models / Hydrogenases / IR spectroscopy / S ligands / Carbonyl ligands

The reactivity of [(μ-X_2bdt)$Fe_2(CO)_6$] [(bdt)**1**, X_2bdt = 3,6-disubstituted bezenedithiolate; X = H, Cl] with ligands of different donor strengths is investigated and compared to that of [(μ-pdt)$Fe_2(CO)_6$] [(pdt)**1**, pdt = propyldithiolate] and [(μ-edt)$Fe_2(CO)_6$] [(edt)**1**, edt = ethyldithiolate]. Strong donor ligands (L = CN^-, PMe_3) when added to (bdt)**1** lead to mononuclear [(bdt)Fe$(L)_2(CO)_2$], (bdt)**6**(L), in a disproportionation and fragmentation reaction, while simple ligand-substitution reactions occur on (edt)**1** and (pdt)**1** under identical conditions. In the presence of weaker ligands such as secondary amines or dmf, the alkyldithiolate-bridged complexes are unreactive, while (bdt)**1** transforms to an O_2-sensitive, magnetically uncoupled species, potentially a mononuclear Fe^I complex coordinated by bdt and at least 2 CO ligands.

Introduction

A class of metalloenzymes termed hydrogenases (H_2ases) is nature's catalysts for the reversible interconversion of protons to molecular hydrogen. Amongst them, [FeFe] H_2ases have been particularly inspirational to bioinorganic chemists, as their active site bears strong resemblance to well-established organometallic iron carbonyls.[1,2] The active site of the enzymes (Figure 1), as deduced by crystallographic[3,4] and spectroscopic studies,[5–8] consists of two low-valent iron centres that are bridged by a non-proteic dithiolate linker. The ligands CO and CN^- occupy most positions of the coordination sphere around the iron centres, supplemented by a cystein-linked [4Fe4S] cluster and a free coordination site that allows for substrate binding.

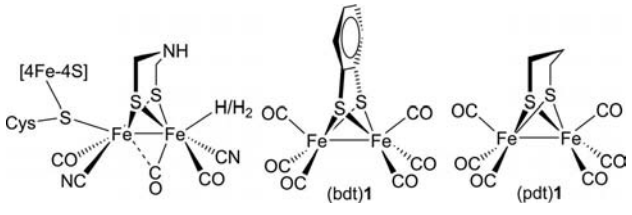

Figure 1. Active site of the [FeFe] hydrogenase and model complexes [(μ-bdt)Fe_2 $(CO)_6$] (bdt)**1** and [(μ-pdt)Fe_2 $(CO)_6$] (pdt)**1**.

Because of the importance of hydrogen as a potential energy carrier of the future,[9,10] a multitude of model complexes of the active site have been reported over the last decade.[11,12] The overall aim of this endeavour is to understand the mode of action of the enzyme and to translate this knowledge into a synthetic catalyst that would catalyze H_2 oxidation and H^+ reduction with a turnover rate and low overpotential similar to the enzymes themselves.[13,14] In this quest, the majority of studies have focussed on the inorganic part of the active site, i.e. the introduction of ligands other than CO that alter the electronic properties of the complexes and can thus give rise to desirable reactivity. Comparably little attention has been given to the organic dithiolate linker that bridges the two iron cations. Most complexes in the literature feature aliphatic dithiolates such as the prototypic propyldithiolate (pdt),[1,15,16] ethyldithiolate (edt)[17] or azadithiolate (adt).[18–20] Unsaturated bridges like benzenedithiolates (bdt)[21–23] and related structures[24,25] have been explored to a much lesser extent.

The differences of aromatically (bdt) relative to aliphatically (such as pdt) bridged complexes are remarkable. The aromatic portion of the bdt delocalizes electron density away from the thiolate groups rendering them weaker donors to the Fe_2 site. As a result, the degree of back-bonding from the metal into the CO-based π* orbitals is less. The iron–carbonyl bond can thus be expected to be weaker and the C=O bond stronger in bdt complexes than those in the pdt analogues. This effect is evidenced by the ν_{CO} frequencies in the IR spectra of [(μ-bdt)$Fe_2(CO)_6$] [(bdt)**1**, Figure 1], which can be observed at higher energies than those of [(μ-pdt)$Fe_2(CO)_6$] [(pdt)**1**, Figure 1].[26] The different electronic impact of the two bridging types is also reflected by the electrochemical behaviour of the complexes. Complex (pdt)**1** is irreversibly reduced at E_{pc} = –1.67 V vs. $Fc^{+/0}$, while (bdt)**1** is reduced at around $E_{1/2}$ = –1.3 V in a reversible two-electron reaction.[22,23] Finally, the thiolates

[a] Department of Photochemistry and Molecular Science
Uppsala University, Box 523, 75120, Uppsala, Sweden
Fax: +46-18-471-6844
E-mail: reiner.lomoth@fotomol.uu.se
sascha.ott@fotomol.uu.se
www.fotomol.uu.se

Supporting information for this article is available on the WWW under http://dx.doi.org/10.1002/ejic.201001152.

of an aromatic bridge can be expected to behave as substantially better leaving groups, potentially facilitating unprecedented ligand-substitution reactions.

Although the above is well established, little work has been done to elucidate whether the aromatic nature of the bridge does lead to different reactivity. To shed light on this, we studied the reactivity of (bdt)**1** towards intermediate-field ligands such as secondary amines or dmf. We showed that the reaction of (bdt)**1** with $HNEt_2$ or dmf gives rise to different products than the analogous reaction of (bdt)**1** with strongly electron-donating CN^- or PMe_3 ligands.[27,28] With (edt)**1** and (pdt)**1**, we verified that alkyldithiolate-bridged complexes are completely unreactive to these intermediate-field ligands and that chelate ring size is irrelevant in this respect.

Results and Discussion

The first step of a ligand-substitution reaction in (pdt)**1** is the addition of an incoming ligand to the Fe^I centre with concomitant change of binding mode of one CO ligand from terminal to bridging [(b)**2**(L) in Scheme 1].[29,30] A similar initial step can be anticipated for (bdt)**1**, by considering the higher electrophilicity of Fe^I in (bdt)**1** relative to that in (pdt)**1**. While the early steps in the two systems are thus independent of the bridging dithiolate, the subsequent steps are very different, as first observed by Rauchfuss et al. ten years ago.[27]

When exposed to 2 equiv. Et_4NCN, (pdt)**1** undergoes simple ligand substitutions reactions to form $[(\mu\text{-pdt})Fe_2(CN)_2(CO)_4]^{2-}$, (pdt)**3**(CN) (pathway A in Scheme 1),[29] whereas an unusual disproportionation reaction is observed for (bdt)**1** under identical reaction conditions (Scheme 1, pathway B). Complex (bdt)**1** fragments and disproportionates to a mononulcear Fe^0 species and an Fe^{II} complex $[(bdt)Fe(CN)_2(CO)_2]^{2-}$, (bdt)**6**(CN).[27] The latter mononuclear species is suggested to be formed via an $[Fe(bdt)(CN)(CO)_2]_2^{2-}$, (bdt)**5**(CN), intermediate that forms from (bdt)**1** already after addition of 1 equiv. CN^-.[27] Intermediate (bdt)**5**(CN) is identical to a crystallographically characterized sample that was prepared by a different route.[31] Complex (bdt)**5**(CN) is coordinatively saturated and is thus expected to be more stable than the 16e$^-$ species (bdt)**4**(CN), which (bdt)**5**(CN) can at least formally be regarded as a dimer of.

The reaction of (bdt)**1** with PMe_3 parallels the analogous reaction with CN^-, but also shows some striking differences. Two types of reaction products are observed with PMe_3: the bis-substituted dinuclear $[(\mu\text{-bdt})Fe_2(PMe_3)_2(CO)_4]$ complex [(bdt)**3**(PMe_3)], but, in analogy to the reaction with CN^-, also the disproportionated mononuclear complex $[(bdt)Fe(PMe_3)_2(CO)_2]$, (bdt)**6**(PMe_3).[28] The ratio between the two products differs somewhat depending on the substituents at bdt. In addition, an Fe^0 species, $[Fe(CO)_3(PMe_3)_2]$, that arises from the disproportionation reaction can be isolated from the reaction mixture. For (bdt)**2**(PMe_3), the rates of CO dissociation and Fe–S cleavage are thus comparable.

From a general viewpoint, (b)**2**(L) can be assumed to be the common intermediate where pathways A and B diverge (Scheme 1). In the case of (pdt)**2**(L), CO dissociation follows the initial ligand association, whereas scission of Fe–S is facilitated and sometimes even dominates for (bdt)**2**(L). The latter reactivity that leads to mononuclear (bdt)**6**(L) can be rationalized by the increased charge delocalization in (bdt)**1**, which renders bdt-S$^-$ a better leaving group than aliphatic pdt-S$^-$. Since *one* CN^- ligand is sufficient to drive the entire fragmentation and disproportionation reaction, the question remains whether the disproportionation drives the fragmentation or whether the formation of a mononuclear species is predominantly facilitated by the special electronic and ligation properties of the bdt ligand. The reactivity of (bdt)**1** towards competing ligands that stabilize higher oxidation states to a lesser extent may provide an answer to this question and at the same time give access to intermediate species between (bdt)**2**(L) and any final products.

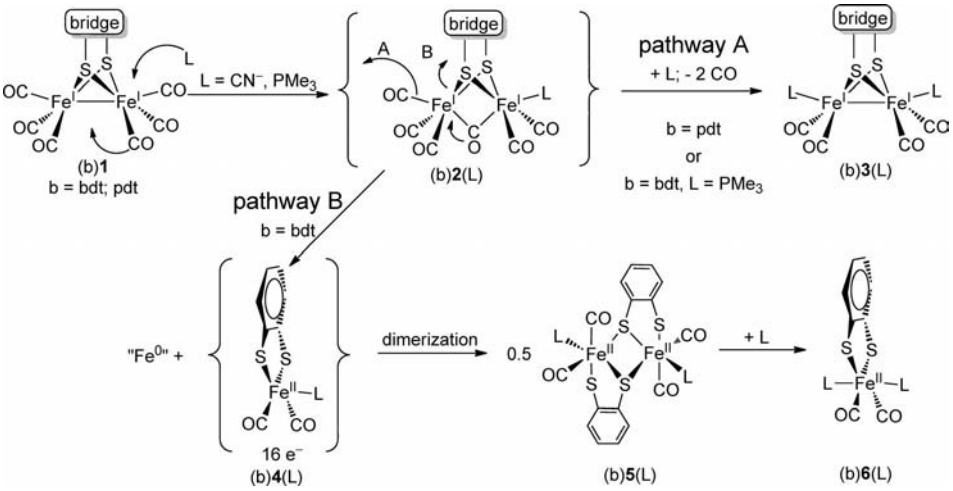

Scheme 1. Different reactivity pathways (A and B) of (bdt)**1** and (pdt)**1**, depending on the incoming ligands and the bridging motif. b = bridge, L = PMe_3 and/or CN^- unless specified differently in the scheme.

We identified the secondary amine $HNEt_2$ as a suitable ligand for this purpose since primary amines have previously been shown to act as decarbonylation agents on (pdt)**1**,[32,33] while tertiary amines may be restricted by too high steric demands. All experiments described hereafter were performed on the 3,6-dichloro-substituted bdt complex [(μ-Cl_2bdt)$Fe_2(CO)_6$], (Cl_2bdt)**1**, because of its reported use in photocatalytic proton reduction schemes.[34]

When $HNEt_2$ is added to a deoxygenated solution of (Cl_2bdt)**1** in CH_3CN at room temperature, a gradual change in colour from red to green can be observed over 1–2 h. UV/Vis absorption spectra of the reaction mixture (Figure 2) show the bleaching of the intense band at 340 nm for (Cl_2bdt)**1** and the concomitant rise of visible absorption below 500 nm and a new band that peaks at 600 nm. One of the initial isosbestic points at 370 nm is not preserved as absorption of the product below 400 nm is lost again in the course of the reaction. The UV/Vis spectra hence suggest that the observed reaction of (Cl_2bdt)**1** with $HNEt_2$ proceeds through two consecutive and kinetically convoluted steps.

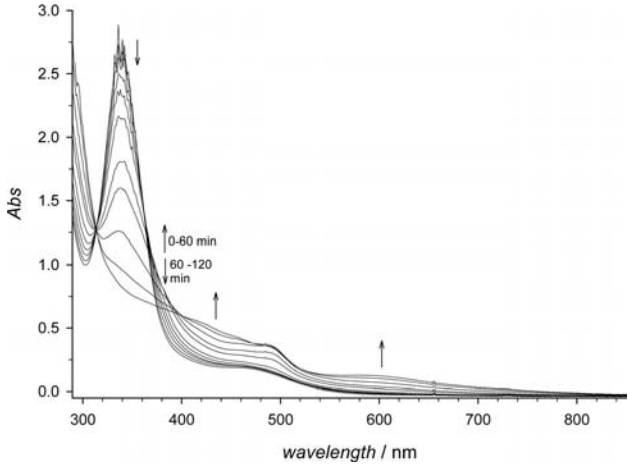

Figure 2. UV/Vis spectra of solutions of 160 μM [(μ-Cl_2bdt)$Fe_2(CO)_6$], (Cl_2bdt)**1**, in deoxygenated CH_3CN after the addition of 0.10 M $HNEt_2$. Arrows indicate directions of spectral changes in time intervals of 12 min.

To obtain information on the products, the reaction of (Cl_2bdt)**1** with $HNEt_2$ was also monitored by IR spectroscopy. In the carbonyl region, the spectrum of (Cl_2bdt)**1** shows three peaks at 2085, 2050 and 2011 cm^{-1}, which slowly decrease after addition of 0.10 M $HNEt_2$ (Figure 3a). After 2 h, the spectrum of the reaction mixture is characterized by mainly two absorption bands at 2018 and 1937 cm^{-1}. The first band strongly overlaps the lowest-energy band assigned to (Cl_2bdt)**1**, and the rise in product absorption is almost fully cancelled by the decrease in reactant absorption. Except for these main product bands and the remaining absorption bands for (Cl_2bdt)**1**, other minor product peaks are observed at 1995 and 1885 cm^{-1}. The peak at 1995 cm^{-1} grows during the first hour but decreases at later times, while the major product peaks still increase. With higher concentration of $HNEt_2$ (Figure 3b), the reaction proceeds more rapidly and almost all (Cl_2bdt)**1** is consumed after only 30 min when the product band at 1995 cm^{-1} reaches its maximum intensity. At later times, this band decays almost completely, in contrast to the main product bands at 2018 and 1937 cm^{-1}. As an additional effect, the higher amine concentration also favours the formation of additional product(s) with bands at 1965 and 1885 cm^{-1}. The IR data hence suggest that the dominating product species (referred to as **7** hereafter) formed in the reaction of (Cl_2bdt)**1** with $HNEt_2$ is characterized by two absorption bands in the carbonyl region at 2018 and 1937 cm^{-1}, while additional bands that can be observed in the course of the reaction presumably arise from intermediates (1995 cm^{-1}) or side products (1965, 1885 cm^{-1}).

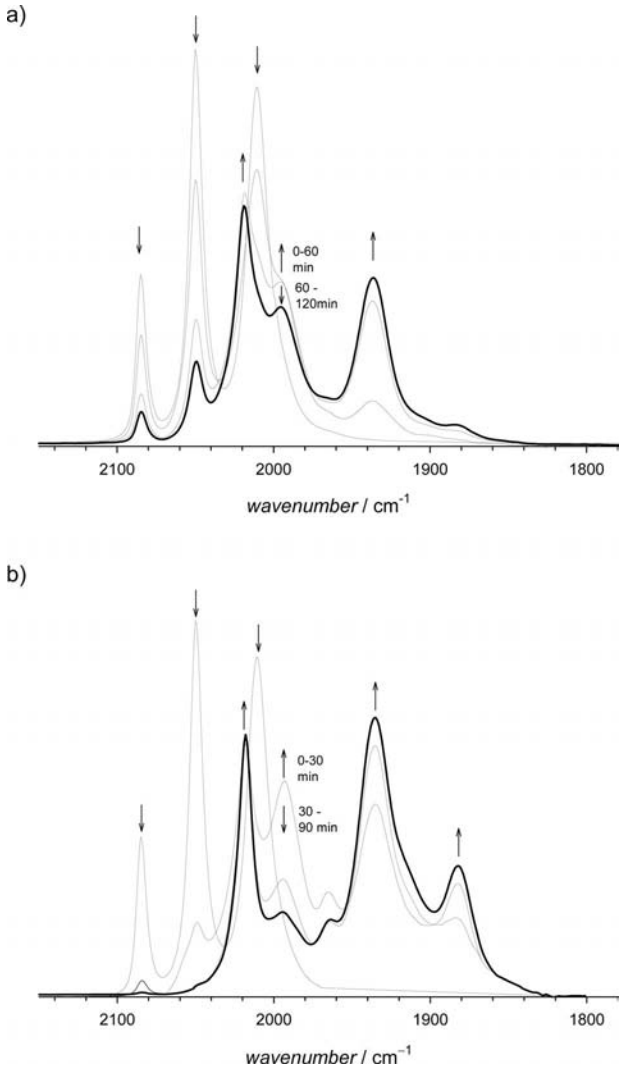

Figure 3. IR spectra of 5 mM [(μ-Cl_2bdt)$Fe_2(CO)_6$], (Cl_2bdt)**1**, in deoxygenated CH_3CN solution, and changes in the spectra after addition of $HNEt_2$. (a) 0.10 M $HNEt_2$; spectra after 0, 20, 60, 120 min. (b) 1.00 M $HNEt_2$; spectra after 0, 30, 60, 90 min.

The two absorption bands of **7** are in a comparable region to those of (bdt)**5**(CN) (2013, 1960 cm^{-1}),[31] (bdt)-**6**(CN) (2006, 2049 cm^{-1})[27] and (bdt)**6**(PMe_3) (2014, 1958 cm^{-1}).[35] However, the two absorption bands in the IR spectrum of **7** are more separated ($\Delta\nu$ = 81 cm^{-1}) than

those of the latter ($\Delta\nu \approx 50$–$60\ cm^{-1}$), which indicates a stronger coupling of the CO ligands in the former.

The formation of **7** is not only triggered by addition of $HNEt_2$ to a CH_3CN solution. When (Cl_2bdt)**1** is dissolved in freshly distilled dmf the colour of the solution changes to green, and changes in the IR spectrum (Figure 4) are very similar to the changes induced by $HNEt_2$ in CH_3CN. The three absorption bands of (Cl_2bdt)**1** (2083, 2048, 2009 cm^{-1}) are replaced by two bands at 2013 and 1932 cm^{-1}. The two bands shift by 5 cm^{-1} to lower wavenumbers in dmf, but have exactly the same separation as that observed in CH_3CN solution. This shift could merely be a solvent effect [cf. the 2-cm^{-1} shift for the parent complex (Cl_2bdt)**1**] or an effect of $HNEt_2$ vs. dmf ligation on **7** and its analogue in dmf solution. The IR spectra indicate that dmf is capable of triggering the same reaction as $HNEt_2$, albeit at a somewhat slower rate.

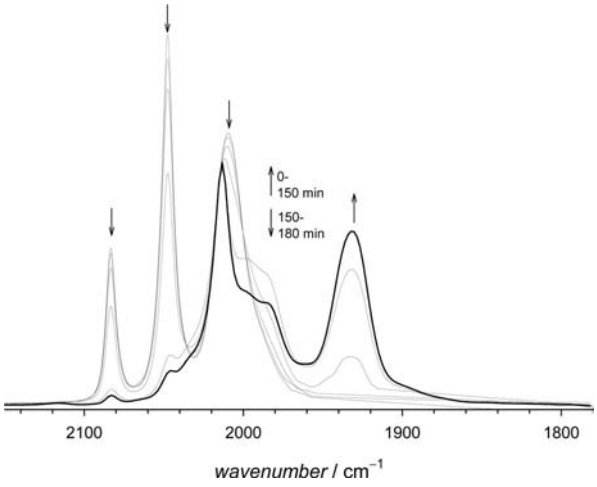

Figure 4. IR spectrum of 5 mM [(μ-Cl_2bdt)$Fe_2(CO)_6$], (Cl_2bdt)**1**, in deoxygenated dmf solution, and changes in the spectrum after 0, 30, 60, 90, 150, 180 min.

Species **7** decomposes instantaneously when exposed to atmospheric oxygen, but slow decomposition also occurs under strict exclusion of oxygen, which renders all attempts of isolation and crystallization futile. The formation of **7** is exclusively observed for the bdt complex, as exposure of (edt)**1** or (pdt)**1** to equivalent conditions has no effect, which leaves the alkyldithiolate-bridged complexes unchanged over hours. It is thus also clear that the reactivity of (Cl_2bdt)**1** is not caused by the five-membered chelate ring.

We recently reported the use of (Cl_2bdt)**1** in a photocatalytic scheme for the generation of hydrogen where dmf had been used as cosolvent.[34] Given the unexpected reactivity of (Cl_2bdt)**1** towards dmf, we were interested in examining whether formation of **7** could have interfered with the catalysis experiments. Under the same conditions of light-driven H_2 evolution and with $Ru(bpy)_3Cl_2$ as photosensitizer and sodium ascorbate as sacrificial donor, (Cl_2bdt)**1** (in CH_3CN) and **7** obtained by reaction with $NHEt_2$, however, gave basically identical rates and turnover numbers for H_2 formation (see Supporting Information).

In attempting to elucidate the role of $HNEt_2$ in the formation of **7**, it was investigated whether $HNEt_2$ can remove a CO ligand on (Cl_2bdt)**1**, similarly to the mode of action of primary amines on (pdt)**1**. If this was the case, the more-established decarbonylation agent trimethylamine-*N*-oxide would be expected to initiate the same chemistry. However, addition of trimethylamine-*N*-oxide to (Cl_2bdt)**1** resulted only in decomposition, but not in the formation of **7**. Decarbonylation of (Cl_2bdt)**1** can thus be excluded as a first step in the mechanism that leads to **7**, and an associative mechanism in which the addition of $HNEt_2$ to (Cl_2bdt)**1** leads to a (Cl_2bdt)**3**($NHEt_2$)-type species seems more likely.

As **7** could only be obtained in situ, we attempted to convert it to a known and stable product. Addition of excess PMe_3 to **7** resulted in a colour change back to red because of the formation of the known mononuclear (Cl_2bdt)**6**(PMe_3) complex, as probed by IR spectroscopy. It is interesting to note that no (Cl_2bdt)**3**(PMe_3) was observed by this route, which is in contrast to the experiment in which PMe_3 was added directly to (bdt)**1**.[28] It is thus tempting to suggest that **7** is a hitherto unknown intermediate between (Cl_2bdt)**2**($NHEt_2$) and **6**(Cl_2PMe_3) along pathway B in Scheme 1.

The reaction of (Cl_2bdt)**1** with $HNEt_2$ is accompanied by the emergence of a signal in the EPR spectrum (Figure 5). The evolution of the EPR signal at approximately $g = 2$ occurs on a similar timescale as the formation of the IR spectrum attributed to **7**. The signal in Figure 5 is the only signal between 50 and 6000 G. Further scans of the signal at a 2-G modulation amplitude continued to show an isotropic signal with no evidence of hyperfine splitting. The signal does not saturate at either low temperature or high power (see Supporting Information), which supports the notion that the observed signal does not result from any sort of organic radical.

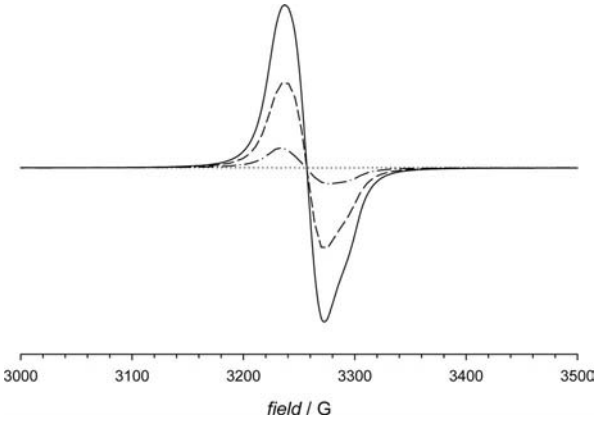

Figure 5. X-band perpendicular mode spectra of a solution of 1 mM [(μ-Cl_2bdt)$Fe_2(CO)_6$], (Cl_2bdt)**1**, in deoxygenated CH_3CN solution after addition of $HNEt_2$ (0.10 M): 0 min (···), 60 min (·-·-), 90 min (---), 120 min (—). All spectra were taken at 15 K temperature and with a 10-G modulation amplitude and 0.02 mW power.

Comparison of the obtained EPR spectrum with that of a mononuclear Fe^I complex from the literature shows that such a complex can be expected to give rise to a signal at

field strengths similar to those observed here.[36] The literature examples, however, exhibit axial or rhombic distortions in comparison to the isotropic nature of our signal, whereas the field strengths and signal widths are comparable. These similarities taken with the temperature and power saturation properties of this signal suggest that the green species contains an iron centre in the oxidation state +1.

The emergence of such an EPR active Fe^{I} species requires major structural changes to break the antiferromagnetic coupling that prevails in dinuclear complexes **1**–**3**. It is clear that this does not occur along pathway A (Scheme 1), where the Fe–Fe distance remains more or less constant. Much larger structural changes occur along pathway B, where (bdt)**5**(L) and mononuclear (bdt)**6**(L) are formed from (bdt)**1** in the presence of strong-field ligands. Considering that such structural changes are also required to explain the magnetically uncoupled Fe^{I} species, it is tempting to assume a similar chemistry for intermediate-field ligands. Mononuclear structures of type **4** or dimeric species such as **5** could account for all spectroscopic data of **7**: a magnetically uncoupled, potentially mononuclear Fe^{I} complex coordinated by at least two CO ligands. From the chemical studies, it can be concluded that the main intermediate also carries the Cl_2bdt ligand since it can be converted to (Cl_2bdt)**6**(PMe_3) by the addition of PMe_3. The exact structure of the green species, however, cannot be deduced from these studies, also because further analysis, for example, by mass spectrometry is inconclusive.

From a general reactivity viewpoint, it seems that the fragmentation that is observed for (bdt)**1** can mostly be attributed to the unique properties of the bdt ligand as it is promoted by both strong- and intermediate-field ligands. The strong ligands are capable of stabilizing the fragmentation products by a subsequent disproportionation that leads to "Fe^{0}" and (bdt)**6**(L) (Scheme 1). In the case of weaker ligands such as amines and dmf, disproportionation is not favoured and the reaction stalls at the stage of the labile Fe^{I} species.

Conclusions

While the dithiolate in model complexes of the active site of the [FeFe] H_2ase is often regarded as a mere structural feature that holds the two Fe centres in place, this work shows that its nature can determine the fate of the compound in ligand-substitution reactions. In the presence of strong donor ligands, (bdt)**1**[37] fragments and disproportionates to (bdt)**6**(L). Exposure of (bdt)**1** to ligands that stabilize higher oxidation states to a lesser extent (secondary amines or dmf) results in the formation of a magnetically uncoupled, potentially mononuclear Fe^{I} species **7** that carries the bdt and CO ligands. Species **7** can be converted into the Fe^{II} complex (bdt)**6**(PMe_3) by addition of PMe_3 and can thus be regarded as an intermediate between (bdt)-**2**(L) and (bdt)**6**(PMe_3). The observation of a magnetically uncoupled Fe^{I} species is indicative of fragmentation being facilitated by the aromatic bridge rather than by disproportionation. Since both (pdt)**1** and (edt)**1** are unreactive towards secondary amines or dmf, effects due to different chelate ring sizes can be ruled out, and the unique electronic and ligation properties of the bdt ligand must be responsible for the substantially richer reactivity of (bdt)**1**.

Experimental Section

Syntheses: The complexes (bdt)**1**, (Cl_2bdt)**1**, (edt)**1** and (pdt)**1** were prepared according to literature methods.[28,38] Identity was verified by elemental analysis, 1D and 2D $^{1}H/^{13}C$ NMR spectroscopy and IR spectroscopy. The decarbonylation agent $Me_3NO{\cdot}2H_2O$ was of reagent grade and was used without further purification. The reaction of (Cl_2bdt)**1** (5 mM) in CH_3CN with Me_3NO (5 equiv.) was conducted in a Schlenk tube under argon atmosphere at room temperature and was monitored by IR spectroscopy. The preparation of (bdt)**6**(PMe_3) via **7** was performed from a solution of (Cl_2bdt)**1** (5 mM) that had been reacted in a Schlenk tube with 1 M $HNEt_2$ in CH_3CN for 1 h under argon atmosphere at room temperature. Subsequently, Me_3P (30 equiv., 1 M in THF, reagent grade) was added, and the reaction was followed by IR spectroscopy.

UV/Vis Spectroscopy: Sample preparation and absorption spectroscopy were performed in a glovebox under argon atmosphere. CH_3CN was of spectroscopic grade and was used as received. Absorption spectra were acquired in a 1-cm pathlength quartz cuvette with an Agilent 8453 UV/Vis spectrophotometer equipped with a fiber-optic coupler to enable measurements inside the glovebox.

IR Spectroscopy: IR absorption spectra were recorded for solutions of the complexes between 4000 and 850 cm^{-1} at a resolution of 1 cm^{-1} on a Bruker (IFS 66 v/S) or a PerkinElmer SpectrumOne FTIR spectrometer in a liquid-sample-cell (Bruker A140) between CaF_2 windows. All reactions with $CH_3CN/HNEt_2$ or dmf were conducted under argon atmosphere by using standard Schlenk techniques with freshly degassed solvents of spectroscopic grade. For IR spectroscopy after different reaction times, samples were transferred from the Schlenk to the liquid-sample-cell, and spectra were acquired immediately after transfer.

EPR Spectroscopy: EPR samples were prepared in a glovebox under argon atmosphere and frozen in liquid nitrogen immediately when taken out of the glovebox. EPR spectra were recorded on a Bruker E500-ELEXYS spectrometer by using an ER 0601SHQE resonator equipped with an ESR900 cryostat and an Oxford ITC503 temperature controller.

Supporting Information (see footnote on the first page of this article): Temperature and power dependence of the EPR signal and photocatalysis experiments.

Acknowledgments

Financial support from the Swedish Research Council (S. O.), the Swedish Energy Agency, the Knut and Alice Wallenberg Foundation, the Wenner Gren Foundation (M. K.) and EU (FP7 Energy 212508 "SOLAR-H2") is gratefully acknowledged.

[1] A. v. F. H. Reihlen, W. Oswald, *J. Liebigs Ann. Chem.* **1928**, 72–96.
[2] C. Tard, X. Liu, S. K. Ibrahim, M. Bruschi, L. D. Gioia, S. C. Davies, X. Yang, L.-S. Wang, G. Sawers, C. J. Pickett, *Nature* **2005**, *433*, 610–613.

[3] J. W. Peters, W. N. Lanzilotta, B. J. Lemon, L. C. Seefeldt, *Science* **1998**, *282*, 1853–1858.
[4] Y. Nicolet, C. Piras, P. Legrand, E. C. Hatchikian, J. C. Fontecilla-Camps, *Structure* **1999**, *7*, 13–23.
[5] C. V. Popescu, E. Münck, *J. Am. Chem. Soc.* **1999**, *121*, 7877–7884.
[6] A. Silakov, E. J. Reijerse, S. P. J. Albracht, E. C. Hatchikian, W. Lubitz, *J. Am. Chem. Soc.* **2007**, *129*, 11447–11458.
[7] A. Silakov, B. Wenk, E. J. Reijerse, W. Lubitz, *Phys. Chem. Chem. Phys.* **2009**, *11*, 6592–6599.
[8] Ö. F. Erdem, L. Schwartz, M. Stein, A. Silakov, S. Kaur-Ghumaan, P. Huang, S. Ott, E. J. Reijerse, W. Lubitz, *Angew. Chem. Int. Ed.*, DOI: 10.1002/anie.201006244.
[9] P. Hoffmann, *Tomorrow's Energy: Hydrogen, Fuel Cells, and the Prospect for a Cleaner Planet*, MIT Press, Cambridge, Massachusetts and London, England, **2002**.
[10] N. Lewis, D. Nocera, *Proc. Natl. Acad. Sci. USA* **2006**, *103*, 15729–15735.
[11] C. Tard, C. J. Pickett, *Chem. Rev.* **2009**, *109*, 2245–2274.
[12] F. Gloaguen, T. B. Rauchfuss, *Chem. Soc. Rev.* **2009**, *38*, 100–108.
[13] J.-F. Capon, F. Gloaguen, P. Schollhammer, J. Talarmin, *Coord. Chem. Rev.* **2005**, *249*, 1664–1676.
[14] G. A. N. Felton, C. A. Mebi, B. J. Petro, A. K. Vannucci, D. H. Evans, R. S. Glass, D. L. Lichtenberger, *J. Organomet. Chem.* **2009**, *694*, 2681–2699.
[15] A. Winter, L. Zsolnai, G. Huttner, *Z. Naturforsch., B* **1982**, *37*, 1430–1436.
[16] M. Y. Darensbourg, E. J. Lyon, J. J. Smee, *Coord. Chem. Rev.* **2000**, *206–207*, 533–561.
[17] J. I. v. d. Vlugt, T. B. Rauchfuss, S. R. Wilson, *Chem. Eur. J.* **2006**, *12*, 90–98.
[18] J. D. Lawrence, H. Li, T. B. Rauchfuss, M. Benard, M.-M. Rohmer, *Angew. Chem.* **2001**, *113*, 1818; *Angew. Chem. Int. Ed.* **2001**, *40*, 1768–1771.
[19] H. Li, T. B. Rauchfuss, *J. Am. Chem. Soc.* **2002**, *124*, 726–727.
[20] S. Ott, M. Kritikos, B. Åkermark, L. Sun, R. Lomoth, *Angew. Chem.* **2004**, *116*, 1024; *Angew. Chem. Int. Ed.* **2004**, *43*, 1006–1009.
[21] J.-F. Capon, F. Gloaguen, P. Schollhammer, J. Talarmin, *J. Electroanal. Chem.* **2004**, *566*, 241–247.
[22] G. A. N. Felton, A. K. Vannucci, J. Chen, L. T. Lockett, N. Okumura, B. J. Petro, U. I. Zakai, D. H. Evans, R. S. Glass, D. L. Lichtenberger, *J. Am. Chem. Soc.* **2007**, *129*, 12521–12530.
[23] J.-F. Capon, F. Gloaguen, P. Schollhammer, J. Talarmin, *J. Electroanal. Chem.* **2006**, *595*, 47–52.
[24] R. J. Wright, C. Lim, T. D. Tilley, *Chem. Eur. J.* **2009**, *15*, 8518–8525.
[25] P. S. Singh, H.-C. Rudbeck, P. Huang, S. Ezzaher, L. Eriksson, M. Stein, S. Ott, R. Lomoth, *Inorg. Chem.* **2009**, *48*, 10883–10885.
[26] L. Schwartz, L. Eriksson, R. Lomoth, F. Teixidor, C. Viñas, S. Ott, *Dalton Trans.* **2008**, 2379–2381.
[27] T. B. Rauchfuss, S. M. Contakes, S. C. N. Hsu, M. A. Reynolds, S. R. Wilson, *J. Am. Chem. Soc.* **2001**, *123*, 6933–6934.
[28] L. Schwartz, P. S. Singh, L. Eriksson, R. Lomoth, S. Ott, *C. R. Chim.* **2008**, *11*, 875–889.
[29] F. Gloaguen, J. D. Lawrence, M. Schmidt, S. R. Wilson, T. B. Rauchfuss, *J. Am. Chem. Soc.* **2001**, *123*, 12518–12527.
[30] S. J. George, Z. Cui, M. Razavet, C. J. Pickett, *Chem. Eur. J.* **2002**, *8*, 4037–4046.
[31] W.-F. Liaw, N.-H. Lee, C.-H. Chen, C.-M. Lee, G.-H. Lee, S.-M. Peng, *J. Am. Chem. Soc.* **2000**, *122*, 488–494.
[32] S. Ott, M. Borgström, M. Kritikos, R. Lomoth, J. Bergquist, B. Åkermark, L. Hammarström, L. Sun, *Inorg. Chem.* **2004**, *43*, 4683–4692.
[33] L. Schwartz, J. Ekström, R. Lomoth, S. Ott, *Chem. Commun.* **2006**, 4206–4208.
[34] D. Streich, Y. Astuti, M. Orlandi, L. Schwartz, R. Lomoth, L. Hammarström, S. Ott, *Chem. Eur. J.* **2010**, *16*, 60–63.
[35] S. Kaur-Ghumaan, L. Schwartz, R. Lomoth, M. Stein, S. Ott, *Angew. Chem. Int. Ed.* **2010**, *49*, 8033–8036.
[36] J. M. Smith, A. R. Sadique, T. R. Cundari, K. R. Rodgers, G. Lukat-Rodgers, R. J. Lachicotte, C. J. Flaschenriem, J. Vela, P. L. Holland, *J. Am. Chem. Soc.* **2006**, *128*, 756–769.
[37] For clarity, no discrimination has been made between bdt and Cl_2bdt in the conclusions.
[38] C. F. Works, *J. Chem. Educ.* **2007**, *84*, 836–838.

Received: October 28, 2010
Published Online: January 26, 2011

